Role of Binding Site Loops in Controlling Nitric Oxide Release: Structure and Kinetics of Mutant Forms of Nitrophorin 4[†,‡]

Estelle M. Maes, Andrzej Weichsel, John F. Andersen,[§] Donald Shepley, and William R. Montfort*

Department of Biochemistry and Molecular Biophysics, University of Arizona, Tucson, Arizona 85721

Received February 3, 2004; Revised Manuscript Received April 2, 2004

ABSTRACT: Nitrophorins are ferric heme proteins that transport nitric oxide (NO) from blood-sucking insects to victims. NO binding is tighter at lower pH values, as found in the insect salivary gland, and weaker at the pH of the victim's tissue, facilitating NO release and subsequent vasodilation. Previous structural analyses of nitrophorin 4 (NP4) from *Rhodnius prolixus* revealed a substantial NO-induced conformational change involving the A−B and G−H loops, which rearrange to desolvate the distal pocket and pack nonpolar residues against the heme-ligated NO. Previous kinetic analyses revealed a slow, biphasic, and pH-dependent NO release, which was proposed to be associated with loop movements. In this study, we created NP4 mutants D30A and D30N (A−B loop), D129A/L130A (G−H loop), and T121V (distal pocket). Eight crystal structures were determined, including complexes with NO, NH_3, and imidazole, to resolutions as high as 1.0 Å. The NO-induced conformational change is largely abolished in the loop mutants, but retained in T121V. Kinetic analyses using stopped-flow spectroscopy revealed the pH dependence for NO release is eliminated for D129A/L130A, considerably reduced for D30A and D30N, but retained for T121V. NO association rates were increased 2−5-fold for T121V, but were unchanged in the loop mutants. Taken together, our findings demonstrate that the pH dependency for NO release is linked to loop dynamics and that solvent reorganization is apparently rate-limiting for formation of the initial iron−nitrosyl bond. Interestingly, the multiphasic kinetic behavior of rNPs was not affected by mutations, and its cause remains unclear.

Nitric oxide (NO)[1] is a second-messenger molecule produced and detected in most if not all higher eukaryotic cells. The list of physiological processes that are regulated by NO continues to grow and includes memory formation, blood coagulation, maintaining correct blood pressure, reproduction, and cell death (*1*, *2*). That NO is central to so many processes is curious, since it is a reactive compound that is toxic at higher concentrations. This property, too, is physiologically important and is used in the immune response by macrophages, for example, to eliminate invading cells. The best characterized NO functions are heme-mediated, yet NO is capable of mediating both heme oxidation and reduction. The compound is produced at the heme center of NO synthase and is detected at the heme center of soluble guanylate cyclase (*3*−*6*). How these activities are accomplished without nonproductive side reactions between heme and NO is not yet understood.

Nitrophorins are heme proteins found in the saliva of certain blood-feeding insects that serve to store NO in the salivary gland and transport and release NO to the tissue of a potential victim, where it induces vasodilation and inhibits blood coagulation (*7*, *8*). *Rhodnius prolixus*, sometimes called the kissing bug, has six such proteins, four originally discovered in the adult insect, which we herein term NP1−4, and two recently discovered nitrophorins, NP5 and NP6, that appear earlier in development (*9*, *10*). The *Rhodnius* nitrophorins are ferric heme proteins that bind NO more tightly at the lower pH of the insect saliva (pH ∼5), where it can be stored on the heme for longer periods without reducing the heme or reacting with oxygen. They assist in blood feeding by delivering NO upon dilution and pH elevation in the host skin, inducing vasodilation in the vicinity of the bite. The nitrophorins also sequester histamine, which is released by the victim in response to the tissue damage caused by the feeding insect (*11*). The rNPs have been well characterized by biochemical (*9*, *12*, *13*), kinetic (*14*−*16*), spectroscopic (*17*, *18*), and crystallographic (*19*−*23*) studies with the aim of understanding the mechanism by which NO is transported, protected, and released to the host (recently reviewed in refs *24* and *25*).

Crystal structures have been determined for three of the six rNPs, NP1, NP2, and NP4 (*19*, *21*, *23*). These studies revealed an overall protein fold containing an eight-stranded β-barrel that is characteristic of the lipocalin family (*23*, *24*).

[†] This work was supported in part by grants from the American Heart Association (E.M.M.) and from the National Institutes of Health (HL62969 to W.R.M. and GM58727 to J.F.A. and W.R.M.).

[‡] Coordinates for all structures reported have been deposited in the Protein Data Bank (PDB entries 1SXU, 1SXW, 1SXX, 1SXY, 1SX0, 1SY1, 1SY2, and 1SY3).

* To whom correspondence should be addressed: Department of Biochemistry and Molecular Biophysics, University of Arizona, 1041 E. Lowell St., Tucson, AZ 85721. Telephone: (520) 621-1884. Fax: (520) 621-1697. E-mail: montfort@email.arizona.edu.

[§] Present address: Laboratory of Malaria and Vector Research, NIAID, National Institutes of Health, 4 Center Dr., Bethesda, MD 20892.

[1] Abbreviations: NO, nitric oxide; rNPs, *Rhodnius* nitrophorins; NP1−6, *Rhodnius* nitrophorins 1−6, respectively; SVD, singular-value decomposition; k_{obs}, individual observed rate constants; k_1, k_{-1} for nitric oxide; k_{1H}, k_{-1H} for histamine; k_{off}, overall dissociation rate constants.

10.1021/bi049748a CCC: $27.50
Published on Web 05/06/2004

Heme is ligated to histidine and centered in one end of the barrel, where numerous van der Waals contacts with nonpolar amino acids lead to a highly nonplanar, ruffled conformation that may be important for setting a reduction potential that favors the ferric (Fe^{3+}) state (*22*, *26*). Ligands bind to the distal side of the heme.

Of particular interest is the crystal structure of the NP4−NO complex at low pH, where a substantial change in the protein conformation is observed (*20*). In the absence of NO, the distal heme pocket is open with the A−B loop (residues 31−37) poorly ordered and the G−H loop (residues 125−133) located away from the heme. When NP4 binds NO, the A−B and G−H loops collapse into the binding pocket, squeezing out solvent and packing nonpolar side chains around the NO moiety. During this event, Asp 30 becomes buried and hydrogen bonded with the Leu 130 carbonyl, while Glu 32, Asp 35, Asp 129, and the N-terminus come together and form an unusual network of hydrogen bonds (Figure 1). NO binding also leads to greater distortion of the heme porphyrin system (*22*). The fact that the NO molecule is packed into a nonpolar pocket and forms no hydrogen bonds with the protein suggests that the NO-induced conformational changes are mediated through hydrophobic interactions.

In kinetic studies of NP1−4, we and others demonstrated that rNPs undergo multiphasic NO interactions. The first phase displays larger association and dissociation rate constants that approach those of metmyoglobin, a protein similar in size and containing the identical heme, while the second phase displays smaller rate constants that are missing in metmyoglobin (*15*, *16*). The rate constants for rNPs fall into two groups that correlate with sequence identity. Rates for NP1 and NP4 are similar, as are those for NP2 (also called prolixin-S) and NP3. The data were interpreted as shown in Scheme 1.

Scheme 1

$$\text{NP} + \text{NO} \underset{k_{-1}}{\overset{k_1}{\rightleftharpoons}} \text{NP-NO} \underset{k_{off1}/k_{off2}\ (\text{pH dep.})}{\overset{k_2}{\rightleftharpoons}} \begin{matrix}\text{NP}'\text{-NO} \\ \text{NP}''\text{-NO}\end{matrix}$$

In this model, there is an initial binding phase (k_1) representing nitrosyl complex formation, with second-order rate constants of ~2 μM^{-1} s^{-1} in NP1 and NP4 (25 °C) and ~30 μM^{-1} s^{-1} in NP2 and NP3 (*15*). This is followed by a lagging first-order phase (k_2) that was estimated to be ~50 s^{-1} in NP2 and suggested to involve protein conformational change. NO release begins with a biphasic, pH sensitive step (k_{off1} and k_{off2}), again suggested to involve the protein conformational change described above, followed by a faster phase (k_{-1}) that was suggested to represent release from the completely open conformation. Measured values for k_{off1} and k_{off2} at pH 5 were ~0.2 and 0.02 s^{-1} for NP1 and NP4 and ~0.05 and ~0.005 s^{-1} for NP2 and NP3, respectively. At pH 8, k_{off1} and k_{off2} increased to ~2 and 0.6 s^{-1} for NP1 and NP4 and to ~0.1 and 0.01 s^{-1} for NP2 and NP3, respectively. Values for k_{-1} were pH-independent: ~5 s^{-1} for NP1 and NP4 and ~40 s^{-1} for NP2 and NP3.

The fact that NO binding is tighter at low pH and induces a closed conformation with a buried carboxylate suggests that loop dynamics may be related to the pH dependence and multiple phases observed in the kinetic measurements.

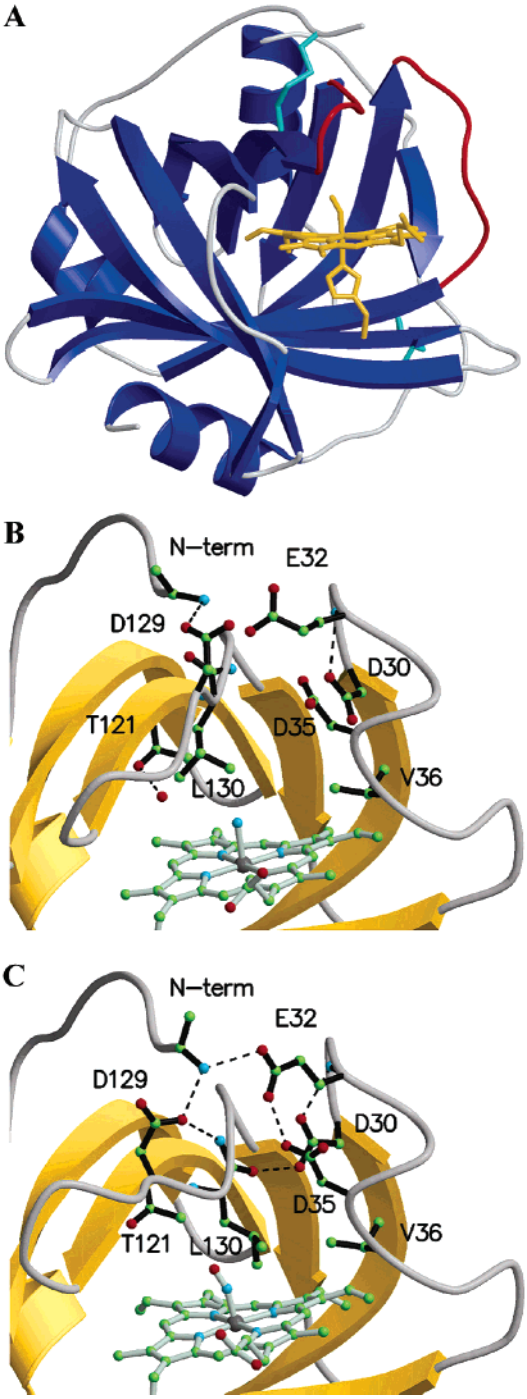

FIGURE 1: Ribbon diagrams of NP4 indicating loops that move on NO binding. (A) Full ribbon drawing of the NP4−NO complex with the A−B and G−H loops highlighted in red. Heme, NO, and His 59 are shown in gold. (B) Close-up of the distal pocket of the NP4−NH_3 complex (open conformation at pH 7.4). Selected residues are shown with ball-and-stick representations (oxygen in red, nitrogen in blue, and carbon in green) and selected hydrogen bonds shown with dashed lines. Residues Glu 32 and Asp 35 are extremely mobile in this complex. Thr 121 occupies the back of the distal pocket and is hydrogen bonded to a water molecule in the open conformer. (C) Close-up of the NP4−NO complex (closed conformation at pH 5.6). Residues Asp 30, Asp 129, and Leu 130, modified in this study, are involved in an extensive hydrogen bond network stabilizing the closed conformer, which includes flipping of the 130−131 peptide bond and new hydrogen bonds to Asp 30 and Asp 129.

Furthermore, little pH dependence is seen in vibrational spectra for the NP1−NO complex (*17*, *18*) or in the heme

reduction potential in NO complexes with NP1−4 (*15*), yet the A−B and G−H loops are highly mobile in the crystal, making it difficult to imagine how they could impede diffusion into and out of the distal pocket. This study was carried out in part to address this quandary.

A second issue arising from the kinetic studies is the basis for the faster association and slower dissociation of NO with NP2 and NP3 than with NP1 and NP4. The distal pocket of NP2 differs in part from those of NP1 and NP4 in that Thr 121, which hydrogen bonds to water in the open conformation in NP1 and NP4, but becomes desolvated in the closed conformation, is an isoleucine in NP2, which leads to a more hydrophobic distal pocket (*19*). Since it appears that the hydrophobicity of NO is key in inducing the closed conformation (*20*), distal pocket solvation and desolvation might be kinetically limiting, a possibility also explored in this work.

Desolvation and protection of a ligand or reaction intermediate, accomplished through conformational changes in mobile loops, are activities common to many proteins, yet the means by which such activities are built into proteins is poorly understood. The rNPs provide an excellent opportunity to investigate such behavior, as well as specific aspects of protein−NO interactions. In this study, we describe the kinetics of the interaction of NO with four mutant forms of NP4: D30N and D30A, which alter the A−B loop; D129A/L130A, which alters the G−H loop; and T121V, which alters the hydrophobicity of the distal pocket (Figure 1). Crystal structures of these proteins, eight in total, are presented to resolutions as high as 1.0 Å. The mutant proteins display structural and kinetic changes consistent with a model in which loop movement and distal pocket desolvation are rate-limiting for NO release.

MATERIALS AND METHODS

Mutagenesis and Expression. NP4 mutants D30A, D30N, D129A/L130A, and T121V were created using PCR and site-directed mutagenesis kits, either the BD Transformer kit from Clontech (D30A and D30N) or the Quick Change kit from Stratagene (D129A/L130A and T121V). The following oligonucleotides purchased from Midland Certified Reagent Co. (Midland, TX) were used as primers: 5′-CAGGTTCCAAAGCTAGGTAATCTG-3′ (D30A), 5′-CAGGTTCCAAGTTTAGGTAATCTG-3′ (D30N), 5′-CTTGGGAGATCTCTACGCTG-3′ (D129A/L130A), and 5′-GCCGCGGGAGATCTCTACGC-3′ (T121V). After mutagenesis and confirmation by DNA sequencing (Arizona Research Laboratories, University of Arizona), the mutants were subcloned into a modified pET17b expression plasmid in which the *Nde*I restriction site was inserted at the beginning of the coding sequence for the NP4 gene, as described previously (*23*). Plasmids pShep205-1, pShep210-3, pCBP49, and pCBP11, carrying the D30A, D30N, D129A/L130A, and T121V mutations, respectively, were transformed into competent *Escherichia coli* BL21(DE3) cells for expression.

Wild-type and mutant proteins were expressed as inclusion bodies, renatured, and purified as described previously (*14*, *20*, *23*). UV−visible absorption spectra of mutants and their NO complexes were identical to those of the wild type (data not shown); unligated proteins exhibited a maximum for the Soret band at 404 nm, and NO derivatives displayed maxima for the Soret, α, and β bands at 419, 568, and 532 nm, respectively.

Kinetics. Kinetic measurements were obtained by rapid-scanning stopped-flow spectrophotometry on an RSM-1000 apparatus (OLIS Inc.). This instrument has a dead time of 2 ms, has a water bath controlled thermostatically to maintain the temperature of the loading syringes and the stopped-flow cell, and is capable of collecting an absorbance spectrum in the visible region every millisecond. In this study, spectra covering a wavelength range of 345−575 nm were measured at 25 °C at a rate of 1000 scans/s, or 62 scans/s for reactions longer than 3 s. Protein solutions (generally ∼1−2 μM for association measurements and 4 μM for histamine displacement measurements), in either 40 mM Tris-HCl (pH 8.0) or sodium acetate (pH 5.0), were deoxygenated with a stream of oxygen-free argon gas before rapid mixing. For NO binding rate measurements, saturated NO buffer solutions (1.9 mM at 25 °C, 1 atm) were diluted in gastight syringes with argon-saturated buffer to produce the desired concentrations. Kinetic data for NO release were measured through displacement with excess histamine, as previously described (*15*).

Data analyses were performed using a singular-value decomposition (SVD) approach and the Global Fitting software provided by OLIS (*27*). Selection of the reaction mechanism was made from evaluation of the fitting residuals and the spectra of reaction intermediates, which are extracted in the SVD approach. In general, reactions for NO association and dissociation were biphasic, as before.

Association Reactions. Association reactions were analyzed according to the reaction illustrated in Scheme 2.

Scheme 2

$$\mathrm{NP + NO} \underset{k_{-1}}{\overset{k_1}{\rightleftharpoons}} \mathrm{NP\text{-}NO} \underset{k_{-2}}{\overset{k_2}{\rightleftharpoons}} \mathrm{NP^*\text{-}NO}$$

In principle, all four rate constants can be obtained from the association data through analyses of the concentration dependence for binding (*28*). In practice, measurement of k_2 is difficult since it is similar in value to k_1[NO], and relatively large. In our analyses, we used an approach that assumes pseudo-first-order conditions for the first step (free ligand concentration unchanging). Where a second phase was indicated, the observed association was fitted to a sequential mechanism, giving rise to k_{obs1} and k_{obs2}. Rate constants k_1 and k_{-1} were obtained through fitting to eq 1 using SigmaPlot (SPSS, Inc., Chicago, IL), where k_{obs1} was the average of three to six shots in the stopped-flow instrument:

$$k_{obs1} = k_1[\mathrm{NO}] + k_{-1} \quad (1)$$

Attempts to obtain k_2 through similar analyses of k_{obs2} were not satisfactory. Therefore, an estimate for k_2 was obtained, where indicated, through fitting of k_{obs2} versus [NO] to a hyperbolic curve, yielding an apparent maximal rate (k_{app2}).

Estimated errors for k_1 and k_{-1} were obtained through averaging of multiple experiments. Accurate measurement of NO concentrations is difficult due to the reactivity and low solubility of the gas, giving rise to increased variability in the measured values. This is especially true for k_{-1}, which is obtained from the *y*-intercept, where small errors produce

large variances. Errors for k_{app2} were also estimated, where possible, from the standard deviation of multiple measurements.

Dissociation Reactions. Estimates of NO release rates were obtained through displacement with excess histamine, which binds tightly to NP4, as previously described (*15*). The analysis requires the rate constant for histamine binding, k_{1H}, which was measured for each protein by stopped-flow spectrophotometry in an approach analogous to that for the NO association measurements. As for NO, histamine binding was found to be biphasic in most cases, and was modeled as such. Measurements were made with an NO concentration of 40 μM and a His concentration of 5 mM and averaged over at least four stopped-flow shots. As before, all displacement reactions were biphasic, giving rise to k_{obs1} and k_{obs2}. NO dissociation rate constants k_{off1} and k_{off2} were calculated with eq 2:

$$k_{obs} = k_{off}/(1 + (k_1[NO]/k_{1H}[His])) \quad (2)$$

We estimated the amplitude of each phase through fitting the absorbance change at a single wavelength to a double exponential, since the Global Fitting software does not provide these values. Errors for histamine association, which is much better behaved than NO association, were estimated from the least-squares fit. Errors for k_{off1} and k_{off2} were estimated from the average of two independent experiments.

Crystallography. Crystals of mutant proteins were grown at room temperature (~25 °C) using the hanging drop technique in either ammonium phosphate (2.8 M, pH 7.5) or PEG 4000 (22%, pH 5.6). All crystals belonged to the *C*2 space group with cell constants typical of those found for wild-type NP4: $a = 74.1$ Å, $b = 42.4$ Å, $c = 52.9$ Å, and $\beta = 94.2°$ (*22*). The NO complexes were obtained by equilibration of a single crystal for 1 h in a precipitant solution saturated with argon followed by soaking for 30 min into a similar solution saturated with NO. A change in color from brown to red, consistent with nitrosylation, was observed during soaking with NO. For data collection, crystals were retrieved with a cryoloop (Hampton) and flash-frozen in liquid nitrogen.

All X-ray diffraction data were recorded at 100 K. Data were acquired with a Rigaku R-AXIS IV^{++} image plate detector associated with a copper rotating anode X-ray source and Osmic mirrors (D30N−imidazole), on beam line 11-1 of SSRL (Stanford Synchrotron Radiation Laboratory, Palo Alto, CA) using a ADSC Quantum 315 detector (D129A/L130A−NH_3), on beam line 9-1 of SSRL with a Mar 345 imaging plate (T121V−NO and D129A/L130A−NO), or on beam line 14BM-D (D30N−NH_3) or 14BM-C (D30N−NO, D30A−NO, and T121V−NH_3) with a Quantum-4 CCD detector of the Advanced Photon Source (Argonne National Laboratory, Argonne, IL). Data were processed with d*TREK (*29*). The initial mutant structures were built using difference Fourier methods and the modeling software O (*30*), starting with the equivalent wild-type NP4 models (PDB entries 1D2U, 1IKJ, and 1KOI for the NH_3, imidazole, and NO complexes, respectively). Models were refined initially with SHELXL (*31*) and subsequently with REFMAC from the CCP4 package (*32*). Certain residues were found to occupy more than one conformation and were built and refined as such. In such cases, the occupancies were generally set to 0.5 for each conformer, and either refined for a few cycles in SHELXL or left fixed when using REFMAC. After completion of the refinement, several cycles of full-matrix refinement using SHELXL (*31*) were performed to estimate the errors for the Fe−distal ligand distance and angle (Table 4). For the full-matrix refinement, the iron coordination sphere (heme, His 59, and NH_3, NO, or imidazole) was completely unrestrained, but all other atoms were fixed. MOLSCRIPT (*33*), BOBSCRIPT (*34*), and RASTER3D (*35*) were used to prepare figures.

RESULTS

To test the role of NP4 A−B and G−H loops in NO binding, release, and pH sensitivity, three mutations were constructed: D30A and D30N in the A−B loop and D129A/L130A in the G−H loop (Figure 1). Asp 30 hydrogen bonds to the carbonyl of Leu 130 in the closed structure, and we hypothesized that the pH dependency for NO release is centered on this interaction (*20*). The Leu 130 side chain moves ~4 Å on binding NO and packs directly against the NO molecule, in an arrangement stabilized in part by a hydrogen bond between Asp 129 and the amino terminus. By removing these interactions, we sought to uncover the relationship between loop movements and kinetics of NO binding and escape.

An additional mutation, T121V, was constructed to test the role of distal pocket hydrophobicity in NO binding and release. Binding of NO to NP2 is faster than to NP4 and release slower, leading to tighter overall binding. One difference between the proteins is that NP2 has an isoleucine at the position equivalent to Thr 121 in NP4, suggesting distal pocket desolvation could play a rate-limiting role in NO affinity.

In what follows, we report the kinetic and structural consequences of these mutations. All four mutations lead to altered structures for ligand complexes and faster NO dissociation.

Kinetics for NO Binding and Release by Wild-Type NP4. Our previous kinetic measurements were obtained through monitoring absorption changes at a single wavelength, 404 or 423 nm, corresponding to the maximum absorption for the unligated protein or the NO complex, respectively (*15*). In the study presented here, we used a stopped-flow device with a shorter dead time (~2 ms) attached to a rapid-scanning spectrophotometer that allowed full spectra (345−575 nm) to be recorded every millisecond. Kinetic rate constants were obtained by simultaneously fitting spectra through a singular-value decomposition (SVD) approach. The absorption spectra for all apparent species in the reaction are extracted in the SVD approach, which aids in the choice of kinetic mechanism. This device and the SVD approach led to increased reliability in our kinetic values, and increased confidence in our choice of kinetic mechanism.

Binding rates were obtained through mixing of NP4 and NO at defined concentrations and monitoring spectral changes. As before, we found the wild-type protein exhibited biphasic NO association (Figure 2). However, unlike in the previous study where the second rate constant could be estimated only for NP2 (*15*, *16*), the approach presented here allowed detection of both k_1 and k_2 for NP4 and its mutant forms, although only an apparent value for k_2 could be reliably obtained (termed k_{app2}; see Materials and Methods).

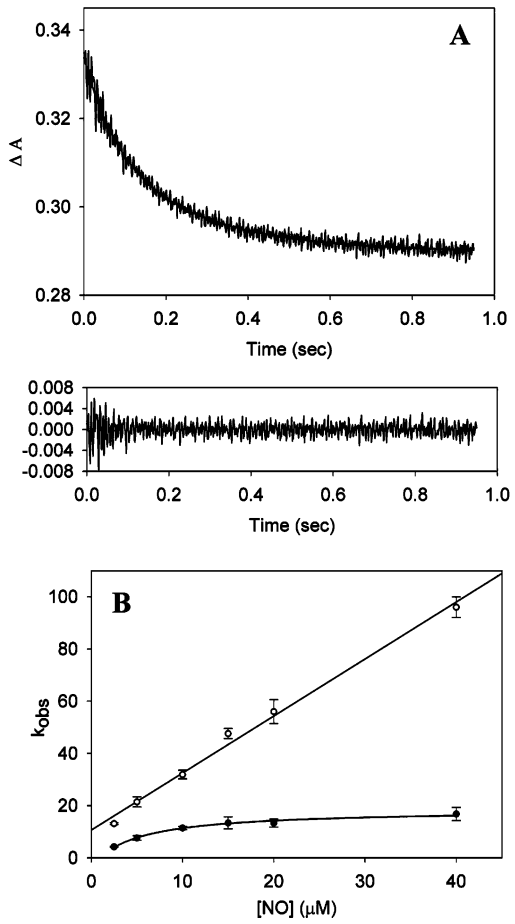

FIGURE 2: Binding of NO to wild-type NP4 detected by rapid mixing at pH 8.0. (A) SVD global fitting of two phases. The residual errors for the fit are shown at the bottom, illustrating good agreement with a biphasic model. (B) NO concentration dependence of k_{obs}. Shown are the average and standard deviation for three measurements of k_{obs} at each NO concentration. Data for the first phase (○) were fitted to eq 1, yielding k_1 and k_{-1}. Data for the second phase (●) were fitted to a hyperbolic curve, yielding a maximal value for the apparent rate constant (k_{app2}).

Dissociation rates were estimated from either the concentration dependence of k_{obs} (k_{-1}; see Methods) or histamine displacement (k_{off1} and k_{off2}), which, as before, were biphasic. Association rate constants for all proteins are shown in Table 1 and dissociation rate constants in Table 2.

NO binding to wild-type NP4 revealed three kinetically distinguishable species (Figure 2A), as previously reported for NP2 (*15*, *16*). The first phase (k_1) exhibited a linear dependence on NO concentration (Figure 2B) and no pH dependence and was in good agreement with previous measurements (*15*). The second phase was saturable and pH-independent and yielded an apparent rate constant similar to those previously measured for NP2 and NP3 (*15*) (Figure 2B).

NO dissociation from wild-type NP4 displayed three kinetically distinguishable species. The faster phase (k_{-1}) was obtained from the binding analyses (eq 1, Figure 2B) and was 3−6-fold larger in this study than in the previous study. As before, k_{-1} was pH-independent. The slower phases (k_{off1} and k_{off2}) were pH-dependent and similar in value to the previous measurements.

The multiphasic kinetic behavior of NP4 indicates the occurrence of intermediate species; however, these species

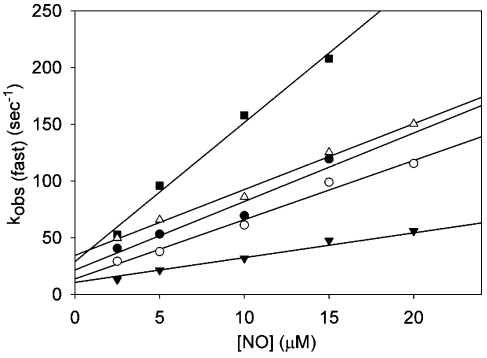

FIGURE 3: NO concentration dependence of k_{obs} (first phase at pH 8) for mutants T121V (■), D30A (△), D30N (●), and D129A/L130A (○) and wild-type NP4 (▼). Each value is the average of two or three measurements.

have absorption spectra that are apparently indistinguishable from those of the final complexes, based on the appearance of isosbestic points in the stopped-flow measurements. Slight nonoverlap in the isosbestic point may indicate a small shift in the intermediate spectra, however.

Kinetics for NO Binding and Release by NP4 Proteins with Loop Mutations. Mutant proteins D30A, D30N, and D129A/L130A, like the wild-type protein, displayed multiphasic kinetics in both the forward and reverse directions, with amplitudes for each phase that were similar to those of the wild type (Tables 1 and 2). Slight increases in k_1 were observed for all three proteins at both pH values that were examined (Figure 3), whereas values for k_{-1}, k_{app2}, and k_{off} (pH 8.0) were unperturbed.

In contrast, both k_{off} phases were larger at pH 5.0 in all three mutant proteins. The wild-type protein displays an ∼21-fold increase in k_{off} between the low and high pH (Table 2). The mutant proteins display k_{off} values at pH 8.0 that are approximately the same as those of the wild type; however, D30A and D30N retain only a slight pH dependence (2−4-fold), and D129A/L130A shows no pH dependence. Thus, the pH dependence for NO release apparently involves the A−B and G−H loop transitions, but the source of multiphasic behavior remains unknown.

Interestingly, histamine binding was also biphasic, which may stem from a stabilization of the histamine complex after formation of four additional hydrogen bonds between the protein and the distal ligand (*15*, *22*). The association rate constants, termed k_{1H} and k_{2H}, were similar for the wild-type protein and mutants D129A/L130A and T121V. However, for D30A and D30N, k_{1H} is 4−5-fold smaller than that of the wild type at pH 8 and k_{2H} 2−3-fold smaller at both pH values. This is likely due to the fact that Asp 30 directly hydrogen bonds to histamine in the complex.

Kinetics for NO Binding and Release by Distal Pocket Mutation T121V. Replacing Thr 121, which hydrogen bonds to a distal pocket water in the open conformation, with a valine affected both association and dissociation reactions (Tables 1 and 2). The value for k_1 increased 3- and 5-fold relative to that of the wild type at pH 5 and 8, respectively, and k_{-1} increased ∼2-fold. In NP2, k_1 and k_{-1} increase between 5- and 20-fold with respect to that of wild-type NP4. Somewhat surprisingly, however, the pH dependency for k_{off} was reduced slightly to ∼7-fold in T121V, displaying slightly smaller rate constants at pH 8.0 but larger rate constants at pH 5.0. Thus, the initial association and dissociation rates

Table 1: NO and Histamine Association Rate Constants for Wild-Type NP4 and NP4 Mutants

	pH 5.0				pH 8.0			
	k_1[a]	k_2[a]	k_{1H}[b]	k_{2H}[b]	k_1[a]	k_2[a]	k_{1H}[b]	k_{2H}[b]
wild-type NP4	2.5 ± 0.6	33 ± 12	0.011 ± 0.003	10 ± 3	2.5 ± 0.4	32 ± 14	4.7 ± 0.2	20 ± 2
D30A	5.2 ± 0.2	21	0.0197 ± 0.0003	nm[c]	6.4 ± 0.9	nm[c]	1.13 ± 0.06	13 ± 2
D30N	6.5 ± 0.9	18	0.022 ± 0.002	3.3 ± 0.5	5.5 ± 0.8	nm[c]	0.97 ± 0.05	18 ± 5
D129A/L130A	4.0 ± 1.5	15 ± 1	0.088 ± 0.004	13 ± 7	4.5 ± 0.9	19 ± 5	3.8 ± 0.3	25 ± 3
T121V	8.1 ± 0.2	27	0.12 ± 0.01	11 ± 2	12.0 ± 4.5	18 ± 0.5	7.9 ± 0.2	28 ± 3

[a] Rate constant for NO (k_1 in μM^{-1} s^{-1} and k_2 in s^{-1}). Standard errors were obtained from two or three replicated sets of measurements. [b] Rate constant for histamine (k_{1H} in μM^{-1} s^{-1} and k_{2H} in s^{-1}). Standard deviations were derived from data fitting. [c] Not measurable.

Table 2: NO Dissociation Rate Constants for Wild-Type NP4 and NP4 Mutants

	pH 5.0				pH 8.0			
	k_{-1}[a]	k_{off1}[b]	k_{off2}[c]	fast[d]	k_{-1}[a]	k_{off1}[b]	k_{off2}[c]	fast[d]
wild-type NP4	21 ± 4	0.15 ± 0.03	0.02 ± 0.0	53	15 ± 7	1.8 ± 0.7	0.6 ± 0.3	59
D30A	17 ± 9	1.3	0.22	58	22 ± 17	2.7 ± 0.3	0.8 ± 0.2	62
D30N	11 ± 10	1.2 ± 0.7	0.14 ± 0.03	56	28 ± 9	2.72 ± 0.03	0.77 ± 0.01	63
D129A/L130A	27 ± 9	1.5 ± 0.3	0.59 ± 0.02	59	27 ± 14	1.9	0.6	58
T121V	44 ± 13	0.39	0.05	56	33 ± 20	1.52 ± 0.09	0.51 ± 0.03	56

[a] Intercept from association data (s^{-1}). Standard errors were obtained from two or three replicated sets of experiments. [b] Fast phase, histamine displacement data (s^{-1}). [c] Slow phase, histamine displacement data (s^{-1}). Standard deviations for the rate constants obtained from the histamine displacement method were derived from two replicated sets of experiments. [d] Percentage of release in the fast phase estimated from fitting single-wavelength (λ = 420 nm) data to a double-exponential equation.

Table 3: X-ray Diffraction Data for NP4 Mutants and Their Complexes

	D30N−NH_3	D30N−Im	D30N−NO	D30A−NO	D129A/L130A−NH_3	D129A/L130A−NO	T121V−NH_3	T121V−NO
pH	7.5	5.6	5.6	5.6	7.0	5.6	7.5	5.6
wavelength (Å)	0.90	1.54	0.90	0.90	0.98	0.75	0.90	0.75
resolution (Å)	20−1.07	19−1.36	11−1.0	22−1.05	26−1.0	31−1.0	21−1.15	31−1.0
total no. of reflections	364789	85068	441539	216051	402050	333593	174365	295229
no. of unique reflections	67346	33304	85604	71942	85962	80684	54132	83307
completeness (%)[a]	98/97	99/96	95/99	98/99	99/99	97/89	97/98	96/89
mean I/σ_I[a]	24.2/9.1	20.3/7.7	17.2/3.5	12.3/2.2	27.3/7.7	18.5/5.2	20.8/6.0	16.6/6.2
R_{sym}[a,b]	0.06/0.20	0.034/0.07	0.07/0.12	0.06/0.26	0.05/0.16	0.05/0.24	0.05/0.13	0.04/0.17

[a] Overall/outermost shell. [b] $R_{sym} = (\sum_h |I_h - \langle I \rangle|)/\sum_h I_h$, where $\langle I \rangle$ is the mean intensity of all symmetry-related reflections I_h.

Table 4: Crystallographic Refinement Statistics and Structural Features

	resolution (Å)	R_{cryst}/R_{free}[a]	Fe−ligand distance (Å)[b]	Fe−ligand angle (deg)	comments
D30N−NH_3	1.07	0.15/0.17	2.04 (2)	n/a[c]	similar to wild type, more solvated
D30N−Im	1.36	0.14/0.18	2.03 (4)	n/a[c]	more open
D30N−NO	1.0	0.14/0.16	1.78 (2)	132 (2)	more open and solvated, ferrous
D30A−NO	1.05	0.15/0.18	1.71 (3)	139 (2)	more open and solvated, ferrous
D129A/L130A−NH_3	1.0	0.16/0.17	2.02 (2)	n/a[c]	similar to wild type, more solvated
D129A/L130A−NO	1.0	0.14/0.15	1.60 (2)	155 (2)	more open and solvated
T121V−NH_3	1.15	0.14/0.17	2.03 (5)	n/a[c]	distal pocket water gone
T121V−NO	1.0	0.13/0.14	1.62 (2)	158 (2)	similar to wild type

[a] $R_{cryst} = (\sum |F_{obs} - F_{calc}|)/\sum F_{obs}$. R_{free} as for R_{cryst}, using a random subset of the data (5%) not included in the refinement. [b] Distance or angle between the heme iron and ligand. Numbers in parentheses are estimated standard deviations calculated after full-matrix refinement of the heme without restraints (see Materials and Methods). [c] Not available.

in T121V, as in NP2, are larger than in wild-type NP4, consistent with solvent reorganization playing a central role in binding and release of NO. The reason for a reduced pH dependence in the mutant protein is not yet clear, but may have to do with a steric clash at low pH (described below).

Crystal Structures. NP4 is the best structurally characterized nitrophorin with crystal structures of complexes with ammonia, water, cyanide, histamine, imidazole, or NO, refined to resolutions as high as 0.85 Å (*20*, *22*, *23*; D. A. Kondrashov and W. R. Montfort, manuscript in preparation). In the study presented here, mutants D30A, D30N, D129A/L130A, and T121V and their complexes with water, ammonia, imidazole, or NO have also been examined by X-ray crystallography, to resolutions between 1.4 and 1.0 Å, and refined to R_{free} values between 0.14 and 0.18 (Tables 3 and 4). Each mutant structure was analyzed with respect to the corresponding wild-type complex, and major changes are listed in Table 4. In addition, the coordination geometry for each structure was refined without restraint so that bond lengths and angles, and their associated errors, could be independently analyzed (Table 4). Certain residues in each complex displayed more than one conformation in the crystal

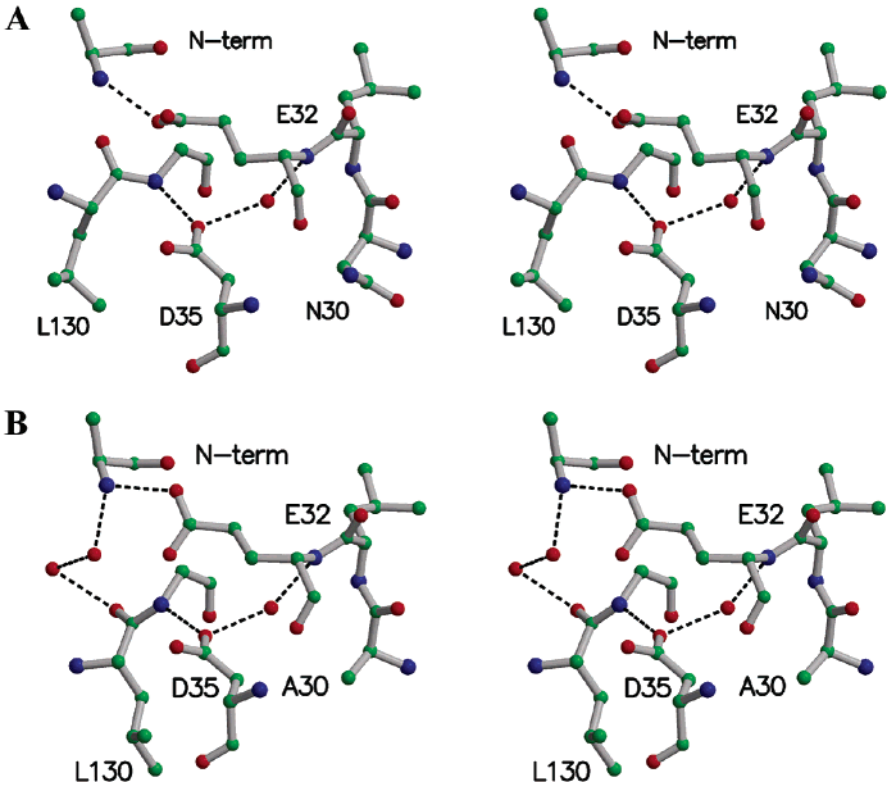

FIGURE 4: Stereoviews of the Asp 30 mutant protein structures. (A) In the D30N−NH_3 complex (pH 7.5), Asn 30 rotates out of the pocket and a new water molecule replaces the wild-type hydrogen bond to the Glu 32 amide. Asp 35 becomes better ordered and directly hydrogen bonded to the Gly 131 amide, which resides in the expected flipped-open conformation. (B) In the D30A−NO complex (pH 5.6), the new water molecule remains in place, as does Asp 35 and the flipped-open conformer of the 130−131 peptide bond, despite NO binding and low pH.

and were modeled as such (up to 11% in the D30N−NO complex). The mutant proteins and their complexes all displayed differences with the wild-type protein.

Structures of Mutants D30A and D30N. In the wild type, one oxygen of the Asp 30 side chain forms a buried hydrogen bond to the Leu 130 carbonyl in the closed conformer, stabilizing the flipped conformer of the 130−131 peptide bond (Figure 1C). The other oxygen forms a hydrogen bond to the backbone amide of Glu 32 in both open and closed conformers. Structures of D30N were determined in complexes with NH_3 (pH 7.5), which is in the open conformation in the wild-type protein; with NO (pH 5.6), which induces the closed conformation in the wild type; and with imidazole (pH 5.6), which also induces closure in the wild-type protein. The structure of the D30A−NO complex (pH 5.6) was also determined.

The D30N−NH_3 structure is very similar to that of the wild-type complex except that Asn 30 rotates out of the distal pocket with respect to the position of Asp 30 in the wild-type protein (Figure 4A). A new water molecule replaces the side of chain of residue 30 in the pocket and hydrogen bonds to the amide of Glu 32 (2.9 Å) and the carboxylate of Asp 35 (2.8 Å). In this arrangement, Asp 35 and the 130−131 peptide are stabilized in the open conformation, with Asp 35 hydrogen bonding to the amide of Gly 131 (2.8 Å), and becoming better ordered than in the wild-type structure.

On binding NO, both D30N and D30A partially close. In the D30A−NO complex (pH 5.6), the new water molecule remains hydrogen bonded to Glu 32 (2.9 Å) and Asp 35 (2.8 Å), and Asp 35 remains hydrogen bonded to Gly 131 (2.8 Å). In this arrangement, the 130−131 peptide bond is prevented from flipping into the closed conformation (Figure 4B), but Leu 130 is still able to move into the distal pocket. In the D30N−NO complex, Asn 30 is able to partially occupy the wild-type position for Asp 30, leading to partial flipping of the 130−131 peptide and hydrogen bonding to carbonyl 130. However, the arrangement is not as stable as in the wild-type protein, and multiple positions for the residues are seen (Figure 5A).

In both D30A−NO and D30N−NO complexes, the Leu 130 side chain moves into the distal pocket and into van der Waals contact with the NO moiety, a shift of several angstroms. The final position for the side chain is very similar to that in the wild-type complex except that the region at the back of the pocket is slightly larger. The distance between Thr 121 and Leu 123 increases by a few tenths of an angstrom, which allows the water molecule near Thr 121 in the open conformation to remain in place in the partially closed D30N− and D30A−NO complexes (Figure 5), whereas this molecule is expelled in the wild-type NO complex (Figure 1). Both NO complexes display geometry consistent with a ferrous iron center (Table 4; see below), indicating photoreduction occurred during measurement.

Structures of Double Mutant D129A/L130A. In the wild-type structure, Asp 129 is weakly associated with the N-terminus and the 130−131 peptide bond is flipped open and weakly associated with solvent. When NO binds, the closed conformation is induced, and the 130−131 peptide bond flips and forms strong hydrogen bonds with Asp 30 and Asp 129. Asp 129 moves ~5 Å and forms strong hydrogen bonds with the N-terminus and the amide of Leu 130, and Leu 130 moves ~4 Å into the distal pocket and

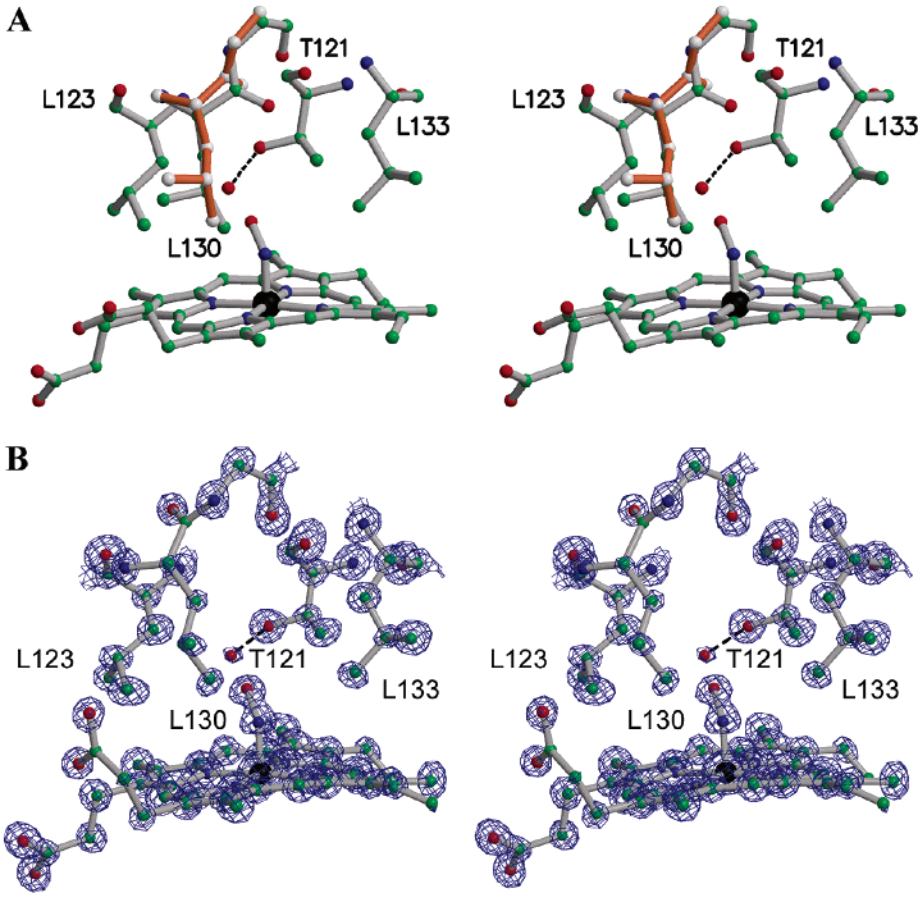

FIGURE 5: Distal pocket in Asp 30 mutant complexes. (A) Stereoview of the D30N−NO complex. Residues 130 and 131 occupy two conformations, shown in gray and orange. Leu 130 is in the closed position in both conformers, despite the 130−131 peptide bond adopting open positions. The more open distal pocket allows the water molecule hydrogen bonded to Thr 121 to remain loosely in place, despite binding of NO. (B) Stereoview of the distal pocket for the D30A−NO complex superimposed with electron density from a $2F_o - F_c$ map contoured at 2.2σ.

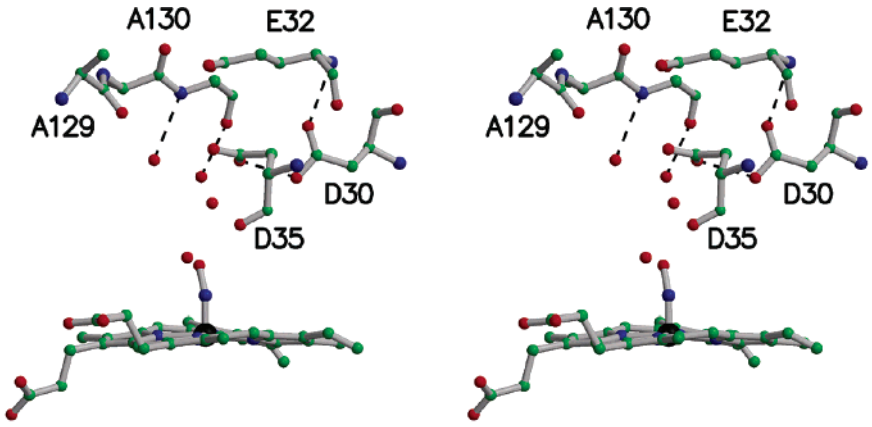

FIGURE 6: Stereoview of the distal pocket of the D129A/L130A−NO complex (pH 5.6). The 130−131 peptide bond is rotated with respect to the wild-type protein, and four new water molecules reside in the more open pocket.

directly contacts NO. The D129A/L130A−NH_3 structure is similar to the wild type except for local changes near the mutation site. In particular, the 129−130 peptide is shifted by ∼2 Å and the Ala 130 side chain is rotated away from the distal pocket, leading to an enlarging of the distal pocket and allowing two or three additional water molecules to bind. The 130−131 peptide bond is rotated ∼90° such that it now forms two new hydrogen bonds, one to the N-terminus (2.6 Å), replacing the hydrogen bond to Asp 129 that was lost to mutation, and another to a new distal pocket water molecule (3.0 Å).

When NO binds, there is little change in the mutation site; however, the A−B loop displays a substantial change. In the binding pocket, the water molecule near the Gly 131 amide remains, along with three other water molecules not found in the wild-type NO complex (Figure 6). The water molecule attached to Thr 121 is lost, however. At the lower pH of the NO structure (5.6), the three carboxylates of Asp 30, Glu 32, and Asp 35 no longer repel one another and are in an arrangement that suggests Asp 30 and Glu 32 are protonated. Asp 30 hydrogen bonds to Asp 35 in the structure (2.6 Å), while Glu 32 hydrogen bonds to carbonyl 130 and

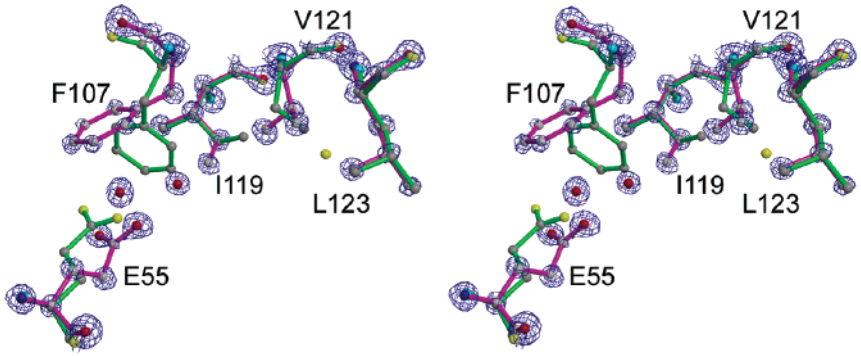

FIGURE 7: Superpositioning of ammonia complexes for the wild type in the B conformation (see the text; green) and T121V (magenta; stereoview). Electron density ($2F_o - F_c$, 3.5σ) is that of the T121V mutant.

is in van der Waals contact with Asp 35 (3.6 Å). In this arrangement, the N-terminus rotates away from carbonyl 130. The structure of the D129A/L130A−NO complex was also examined at pH 7.0 to 1.4 Å and is similar to that obtained at pH 5.6 (data not shown).

Structures of Mutant T121V. Two structures of T121V were determined and found to be nearly identical to their wild-type counterparts. In both T121V−NH_3 and T121V−NO complexes, Val 121 is rotated by ~100° with respect to Thr 121, inducing a repacking of Glu 55, Phe 107, and Ile 119, the latter of which contacts this group (see below; Figure 7). The water molecule that exits on NO complex formation in the wild-type protein is not found in the mutant protein.

In the wild-type protein, Glu 55, Phe 107, and Ile 119 can occupy two positions, one in which Phe 107 swings to one side, allowing buried Glu 55 to become solvated with two interior water molecules (conformer A), and one in which Phe 107 swings into contact with Glu 55, expelling the two water molecules (conformer B). The A conformation is favored by higher pHs, warmer temperatures, and hydrophilic ligands, whereas the B conformation is favored by low pHs, frozen states, and NO ligation (*19*, *22*, *23*; D. A. Kondrashov and W. R. Montfort, manuscript in preparation; C. Punchihewa, E. M. Maes, and W. R. Montfort, manuscript in preparation). No functional consequences have been attributed to these changes to date, and the E55Q mutant protein behaves like the wild type (C. Punchihewa, E. M. Maes, and W. R. Montfort, manuscript in preparation). In the study presented here, the T121V−NH_3 complex completely resides in the A conformation, which relieves the steric conflict between Ile 119 and Val 121, whereas the wild type is observed in both A and B conformations. The T121V−NO complex completely resides in the B conformer, but is slightly distorted due to steric conflict between Ile 119 and Val 121, which leads to an ~0.2 Å distortion in the closest pyrrole ring of the heme.

Ferric versus Ferrous Nitrosyl Complexes. Metal centers in proteins are prone to photoreduction in the intense X-ray sources available at synchrotrons (*36*). The wild type and the mutant forms of NP4 used in this work were all in the ferric state when crystallized; however, the D30A−NO and D30N−NO structures display geometry consistent with ferrous complexes (Table 4), suggesting photoreduction occurred during data measurement. The initial protein conformation, preserved upon flash-freezing of the crystal, is not altered by photoreduction. More broadly, structures of the chemically reduced NP4−NO complex display the same closed conformation as the oxidized form (E. M. Maes and W. R. Montfort, manuscript in preparation). However, photoreduction in NP4 leads to Fe−NO bond lengths that are longer (~1.7 Å vs ~1.6 Å) and more bent [~140° vs ~160° (*22*)], differences that require high resolution for detection. In wild-type NP4, photoreduction is correlated with more solvated distal pockets and the use of longer-wavelength X-rays, parameters that may affect the generation and flow of hydrated electrons. Thus, the low-pH NP4−NO structures determined with shorter-wavelength X-rays, which exhibit stable closed conformers, are ferric (*22*), while the high-pH NP4−NO structure, which exhibits multiple conformers, is ferrous (D. A. Kondrashov and W. R. Montfort, manuscript in preparation). This trend is also seen in the structures described herein, in which the more open structures (D30N and D30A) are photoreduced while the more closed (T121V) is not. The exception to this trend is the D129A/L130A−NO structure, which is ferric but exhibits an open conformer. The lack of photoreduction in this case is possibly related to the very short wavelength X-rays (0.75 Å) used in the structure determination.

DISCUSSION

The primary functions of nitrophorins are to store, transport, and release NO, a small, highly diffusible, and reactive molecule. Our previous studies suggest that this is accomplished through simple gating using highly mobile distal pocket loops, a mechanism that is surprising in that highly mobile loops are generally transparent to small molecule diffusion. In this study, we test this possibility through mutation, kinetic, and crystallographic studies. We also test the role of distal pocket desolvation in kinetic events. The results confirm that both loop dynamics and distal pocket solvation are important in NO binding and release.

Role of Binding Site Loops in Regulating NO Release. Two loops, the A−B loop and the G−H loop (Figure 1), undergo substantial changes in conformation on binding NO, leading to a structure with a complicated hydrogen bonding arrangement near the distal pocket, and a desolvated, hydrophobic arrangement in the distal pocket. These loops were targeted for mutation in this study. Mutations D30A and D30N alter a key hydrogen bond in the closed conformer, and the double mutation D129A/L130A alters both a key hydrogen bond and a key van der Waals contact with the NO moiety. Strikingly, all three mutants have lost the high-affinity state for NO binding that occurs at low pH, displaying almost no pH dependence for release. Yet, to our surprise, all three

mutant proteins retain the unusual multiphasic binding and release kinetics characteristic of the *Rhodnius* nitrophorins, and display release rates that are no faster than those of the wild type at pH 7.4, which in itself is relatively slow.

Ultra-high-resolution crystal structures of the mutant proteins are consistent with the kinetic results. In all three NO complexes at low pH, the A−B and G−H loops adopt conformations more open than those found in the wild-type complex. In the D30N−NO and D30A−NO complexes, Leu 130 still moves into the distal pocket and contacts NO, and perhaps this event is somehow pH sensitive and gives rise to the small residual pH dependence for NO release that the D30 mutants retain. However, the D129A/L130A double mutant, which has completely lost this van der Waals contact with NO, has release rates that are no faster than those of the wild type at pH 7.4, suggesting that the Leu 130 side chain is not an impediment to release unless stabilized through the other loop hydrogen bonds.

The fact that NO diffusion out of the distal pocket is facilitated in proteins with destabilized loop conformations suggests that binding site loop opening does indeed regulate the release of NO, and that rate constants k_{off1} and k_{off2} reflect rates for loop dynamics, as we have previously proposed (*15*). However, since all of the mutants retain multiphasic kinetics, either additional loop movements into and out of the pocket are functionally important or some other factor is at play. One possibility is that Val 36, a residue that packs against NO, and the 130−131 peptide bond, which can flip between open and closed conformers, are influencing release. In this study and in structures of wild-type NP4 recently determined at 0.85 Å resolution (D. A. Kondrashov and W. R. Montfort, manuscript in preparation), it has become clear that Val 36 partially occupies the closed conformation under all conditions favoring the open conformation (ligand-free low-pH, ligand-free high-pH, and NO-bound high-pH conditions). Likewise, the 130−131 peptide bond can occupy more than one conformation under a given set of conditions (see, for example, Figure 5). Variability in the structure of the distal pocket may very well cause the NO ligand to be distributed differently as it diffuses through the pocket. An alternative possibility for the multiphasic kinetics could be multiple forms of the nitrosyl complex with multiple Fe−NO bond strengths. This explanation seems unlikely on the basis of Raman spectroscopic measurements with NP1 (*18*) and NP4 (A. Zareba and R. S. Czernuszewicz, personal communication). However, the facts that two NO stretching frequencies are seen for the NP1−NO complex (*17*) and the Fe−NO bond in ultra-high-resolution structures of NP4 is clearly distorted (*22*) suggest multiple cleavage rates of the Fe−NO bond may exist.

Role of Distal Loops in the pH Sensitivity. Earlier studies of insect-derived and recombinant rNPs showed the NO release to be slower at the pH of the insect saliva (∼5) than at the physiological pH of the host (∼7.4), a requirement for stable storage of NO in the insect salivary gland and release of NO into the victim, yet the relationship between the release rates and the pH sensitivity had not been established. The transition between high and low affinity follows a path consistent with titration of a single group with an apparent pK_a of 6.5 (*15*). We have previously suggested this group could belong to either Asp 30, which forms a buried hydrogen bond in the closed conformer [Figure 1 (*20*)], or Glu 55, which is located in the protein interior, is conserved, and displays a pH-dependent change in solvation (*23*). Glu 55 now appears not to be involved since the mutant E55Q is structurally and kinetically identical to the wild-type protein (C. Punchihewa, E. M. Maes, and W. R. Montfort, manuscript in preparation). However, the work presented here is consistent with burial of Asp 30 in the pH sensitive step, since D30A and D30N mutant proteins display minimal pH dependence for NO release, although the residual pH sensitivity for NO release, ∼4% of that of the wild type, suggests that other factors are involved in a minor way. The double mutant D129A/L130A completely lost its pH dependence; however, it was locked into a conformation in which the Asp 30 hydrogen bond to the Leu 130 carbonyl in the closed conformer could not occur (Figure 6). The kinetic and structural results, taken together, suggest that the pH dependency for NO release is due to changes in loop dynamics. The wild-type NP4−NO structures at pH 5.6 (*20*) and pH 7.5 (D. A. Kondrashov and W. R. Montfort, manuscript in preparation) are consistent with the mutagenesis results: at higher pH the hydrogen bonding network stabilizing the closed conformation (Figure 1) is largely disrupted.

Role of Distal Pocket Hydrophobicity in NO Affinity. From the foregoing, it seems clear that the rate-determining step for NO release at low pH involves loop disordering. But what of the driving force for loop closure? Previous studies have suggested that it is the hydrophobicity of NO that is sensed (*20*). Complexes with cyanide and ammonia do not induce the closed conformer, even at low pH, whereas complexes with NO (70 times more soluble in hexane than water) partially induce closure at pH 7.4, and completely induce closure at pH 5.6. Added to this is NP2, which binds NO more tightly than NP4, displays both faster association (k_1) and slower dissociation (k_{off}) than NP4, and has a more hydrophobic pocket than NP4 (*15*, *19*). In particular, residue Thr 121, which lies at the back of the distal pocket in NP4 and orders a water molecule near the NO binding site, is replaced with Ile 120 in NP2, with the concomitant loss of the ordered water molecule.

The mutant NP4 protein T121V displays some properties similar to those of NP2, and others not. The structure of the T121V−NH_3 complex has indeed lost the ordered water molecule near the NO binding site; the only other visible effect is to shift the equilibrium between two possible conformations for residues Glu 55, Phe 107, and Ile 119 to one with better solvation of Glu 55. Likewise, the T121V−NO complex is quite similar to the wild-type complex, except for the repacking of Phe 107 and Ile 119 into a slightly shifted arrangement. However, in the closed complex of the mutant, the heme pyrrole ring nearest the mutation site, which contacts all three residues that move (Val 121, Phe 107, and Ile 119), is shifted toward the proximal side by ∼0.2 Å, giving rise to a slightly more distorted heme than in the wild-type protein. Kinetically, T121V has larger values for both k_1 and k_{-1}, representing the first binding and last release steps in our kinetic model, respectively. A similar effect also occurs in NP2, but to an even greater extent (2−4-fold greater in NP2 than in T121V). This is consistent with the initial NO association and dissociation rates being coupled to desolvation rates. However, the values for k_{off} at low pH were slightly larger in T121V than in wild-type NP4, unlike the

case for NP2. A possible explanation for this is that the closed conformation is less stable in the mutant protein, due to the increase in heme distortion near the mutation site.

Interestingly, NO association is also slightly faster for mutants D30A, D30N, and D129A/L130A. The distal cavities for these mutants are less encumbered than in the wild type, suggesting that greater accessibility of the binding site can also lead to faster NO association.

Mechanistic Steps Involved in NO Binding and Release. The linking of protein dynamics to solution kinetics is a challenging task. Our working model for rNP has NO binding to a relatively open distal pocket (k_1) followed by loop closure (k_2, Scheme 2). NO release proceeds in reverse in this model, with loop opening (k_{-2}) preceding NO release (k_{-1}). Support for this model comes from the NO-induced conformational change found for NP4; the demonstration of biphasic binding behavior in NP1−4 under a variety of conditions (*15*, *16*), with the second phase ranging in NP4 from 10 to 60% of the total signal; the detection of slower (k_{off}) and faster (k_{-1}) release phases; and the comparison of NO dissociation constants with rate constants, which are consistent with the biphasic working model [i.e., $K_d \approx k_{-2}/k_1$ (*15*)]. That the first association phase is due to ligand binding rather than a protein conformation change is suggested by the open binding pocket in the unliganded structure, and the different values for k_1 obtained with different ligands (e.g., cyanide binds ∼1000 times slower at pH 8.0 than NO; E. M. Maes and W. R. Montfort, unpublished observation). In contrast, the rate-limiting step in ligand binding to cytochromes *c* and c_2 is a protein conformational change, leading to similar binding rates for all ligands and nonlinear plots of k_{obs} versus ligand concentration (*37*, *38*). Despite these features, the model described in Scheme 1 is clearly inadequate for describing all of the kinetic data. The slower release phase is itself biphasic, which we term k_{off1} and k_{off2} (Scheme 2), and is pH sensitive, whereas neither observed association phase is pH sensitive.

These studies with NP4 allow us to begin linking protein dynamics to solution kinetics. The pH dependence for NO release is clearly related to loop displacement, since this feature was disrupted in all of the A−B and G−H mutants, both structurally and kinetically. Solvent reorganization is apparently rate-limiting for the formation of the initial iron−nitrosyl bond, since the T121V mutation leads to disordering of the solvent structure in the distal pocket, and to an increase in k_1. It is tempting to speculate that the second kinetic phase in binding that we detect (k_2) is related to loop reordering; however, nothing we have varied (pH or mutations) has led to a detectable change in this phase, despite quite different resulting structures. Thus, it remains unclear what this phase represents, although it may be related to Val 36 and the 130−131 peptide bond, both of which occupy multiple conformations in the unliganded protein and thus could lead to more than one entry path.

NO release displays the most pronounced pH dependence, and this dependence can be completely eliminated through mutation of the A−B and G−H loops. Thus, the most mobile parts of the protein can have a strong effect on NO release. This step (k_{off}) is also biphasic, both components of which are affected by changes in loop dynamics through pH or mutation. As with k_2, the reason for this biphasic behavior is unclear, only that it likely involves the loops. The final release phase (k_{-1}) is sensitive to factors that lead to greater solvent dynamics, consistent with the model in which it represents release from the open pocket.

Binding of NO and other diatomic ligands to ferric (met)-myoglobin is faster than to the rNPs and monophasic, despite the blockage of the binding pocket by a histidine. For example, k_{on} for NO binding by elephant metmyoglobin equals 22 μM^{-1} s^{-1}, ∼10-fold larger than that for NP4, and k_{off} = 40 s^{-1}, 20−2000-fold larger than that for NP4, depending on pH and phase (*39*). The rNPs and myoglobins are approximately the same size and contain the same heme group, yet the rNPs have evolved an ability to regulate NO diffusion and reduce NO side reactions that is not present in the globins, and have done so with a large distal pocket and two highly mobile loops. The complete understanding of how this is accomplished remains to be discovered, but it is intricately linked to protein dynamics, solvent dynamics, and heme distortion, areas of intense investigation for the general understanding of protein function.

ACKNOWLEDGMENT

We thank Carrie Plummer for her assistance in mutant and protein preparation and Abreeza Zegeer for her assistance with crystal growth. Portions of this research were carried out at the Stanford Synchrotron Radiation Laboratory, a national user facility operated by Stanford University on behalf of the U.S. Department of Energy. Diffraction data were also measured at BioCARS Sector 14, Advanced Photon Source, Argonne National Laboratory, which was supported by the U.S. Department of Energy under Contract W-31-109-Eng-38. Use of BioCARS Sector 14 was supported by the National Institutes of Health, National Center for Research Resources, under Grant RR07707.

REFERENCES

1. Moncada, S., and Erusalimsky, J. D. (2002) Does nitric oxide modulate mitochondrial energy generation and apoptosis? *Nat. Rev. Mol. Cell Biol. 3*, 214−220.
2. Bredt, D. S., and Snyder, S. H. (1994) Nitric oxide: A physiologic messenger molecule, *Annu. Rev. Biochem. 63*, 175−195.
3. Stuehr, D. J. (1999) Mammalian nitric oxide synthases, *Biochim. Biophys. Acta 1411*, 217−230.
4. Denninger, J. W., and Marletta, M. A. (1999) Guanylate cyclase and the •NO/cGMP signaling pathway, *Biochim. Biophys. Acta 1411*, 334−350.
5. Koesling, D. (1999) Studying the structure and regulation of soluble guanylyl cyclase, *Methods 19*, 485−493.
6. Ludwig, M. L., and Marletta, M. A. (1999) A new decoration for nitric oxide synthase: a Zn(Cys)4 site, *Struct. Folding Des. 7*, R73−R79.
7. Ribeiro, J. M. C., Hazzard, J. M. H., Nussenzveig, R. H., Champagne, D. E., and Walker, F. A. (1993) Reversible binding of nitric oxide by a salivary heme protein from a bloodsucking insect, *Science 260*, 539−541.
8. Valenzuela, J. G., and Ribeiro, J. M. C. (1998) Purification and cloning of the salivary nitrophorin from the hemipteran *Cimex lectularius*, *J. Exp. Biol. 201*, 2659−2664.
9. Champagne, D. E., Nussenzvieg, R. H., and Ribeiro, J. M. C. (1995) Purification, partial characterization and cloning of nitric oxide-carrying heme proteins (nitrophorins) from salivary glands of the blood-sucking insect *Rhodnius prolixus*, *J. Biol. Chem. 270*, 8691−8695.
10. Moreira, M. F., Coelho, H. S., Zingali, R. B., Oliveira, P. L., and Masuda, H. (2003) Changes in salivary nitrophorin profile during the life cycle of the blood-sucking bug *Rhodnius prolixus*, *Insect Biochem. Mol. Biol. 33*, 23−28.
11. Ribeiro, J. M. C., and Walker, F. A. (1994) High affinity histamine-binding and antihistaminic activity of the salivary nitric oxide-

carrying heme protein (nitrophorin) of *Rhodnius prolixus*, *J. Exp. Med. 180*, 2251−2257.
12. Sun, J., Yuda, M., Miura, K., and Chinzei, Y. (1998) Characterization and cDNA cloning of a hemoprotein in the salivary glands of the blood-sucking insect, *Rhodnius prolixus*, *Insect Biochem. Mol. Biol. 28*, 191−200.
13. Sun, J., Yamaguchi, M., Yuda, M., Miura, K., Takeya, H., Hirai, M., Matsuoka, H., Ando, K., Watanabe, T., Suzuki, K., and Chinzei, Y. (1996) Purification, characterization and cDNA cloning of a novel anticoagulant of the intrinsic pathway (prolixin-S) from salivary glands of the blood sucking bug, *Rhodnius prolixus*, *Thromb. Haemostasis 75*, 573−577.
14. Andersen, J. F., Champagne, D. E., Weichsel, A., Ribeiro, J. M. C., Balfour, C. A., Dress, V., and Montfort, W. R. (1997) Nitric oxide binding and crystallization of recombinant nitrophorin I, a nitric oxide transport protein from the blood-sucking bug *Rhodnius prolixus*, *Biochemistry 36*, 4423−4428.
15. Andersen, J. F., Ding, X. D., Balfour, C., Shokhireva, T. K., Champagne, D. E., Walker, F. A., and Montfort, W. R. (2000) Kinetics and equilibria in ligand binding by nitrophorins 1−4: Evidence for stabilization of a NO-ferriheme complex through a ligand-induced conformational trap, *Biochemistry 39*, 10118−10131.
16. Kaneko, Y., Yuda, M., Iio, T., Murase, T., and Chinzei, Y. (1999) Kinetic analysis on nitric oxide binding of recombinant Prolixin-S, a nitric oxide transport protein from the bloodsucking bug, *Rhodnius prolixus*, *Biochim. Biophys. Acta 1431*, 492−499.
17. Ding, X. D., Weichsel, A., Andersen, J. F., Shokhireva, T. K., Balfour, C., Pierik, A. J., Averill, B. A., Montfort, W. R., and Walker, F. A. (1999) Nitric oxide binding to the ferri- and ferroheme states of nitrophorin 1, a reversible NO-binding heme protein from the saliva of the blood-sucking insect, *Rhodnius prolixus*, *J. Am. Chem. Soc. 121*, 128−138.
18. Maes, E. M., Walker, F. A., Montfort, W. R., and Czernuszewicz, R. S. (2001) Resonance Raman spectroscopic study of nitrophorin 1, a nitric oxide-binding heme protein from *Rhodnius prolixus*, and its nitrosyl and cyano adducts, *J. Am. Chem. Soc. 123*, 11664−11672.
19. Andersen, J. F., and Montfort, W. R. (2000) Crystal structures of nitrophorin 2: A trifunctional antihemostatic protein from the saliva of *Rhodnius prolixus*, *J. Biol. Chem. 275*, 30496−30503.
20. Weichsel, A., Andersen, J. F., Roberts, S. A., and Montfort, W. R. (2000) Reversible nitric oxide binding to nitrophorin 4 from *Rhodnius prolixus* involves complete distal pocket burial, *Nat. Struct. Biol. 7*, 551−554.
21. Weichsel, A., Andersen, J. F., Champagne, D. E., Walker, F. A., and Montfort, W. R. (1998) Crystal structures of a nitric oxide transport protein from a blood-sucking insect, *Nat. Struct. Biol. 5*, 304−309.
22. Roberts, S. A., Weichsel, A., Qiu, Y., Shelnutt, J. A., Walker, F. A., and Montfort, W. R. (2001) Ligand-induced heme ruffling and bent NO geometry in ultra-high resolution structures of nitrophorin 4, *Biochemistry 40*, 11327−11337.
23. Andersen, J. F., Weichsel, A., Balfour, C. A., Champagne, D. E., and Montfort, W. R. (1998) The crystal structure of nitrophorin 4 at 1.5 Å resolution: Transport of nitric oxide by a lipocalin-based heme protein, *Structure 6*, 1315−1327.
24. Montfort, W. R., Weichsel, A., and Andersen, J. F. (2000) Nitrophorins and related antihemostatic lipocalins from *Rhodnius prolixus* and other blood-sucking arthropods, *Biochim. Biophys. Acta 1482*, 110−118.
25. Walker, F. A., and Montfort, W. R. (2000) in *Advances in Inorganic Chemistry* (Mauk, G., and Sykes, A. G., Eds.) pp 295−358, Academic Press, San Diego.
26. Shokhireva, T., Berry, R. E., Uno, E., Balfour, C. A., Zhang, H., and Walker, F. A. (2003) Electrochemical and NMR spectroscopic studies of distal pocket mutants of nitrophorin 2: stability, structure, and dynamics of axial ligand complexes, *Proc. Natl. Acad. Sci. U.S.A. 100*, 3778−3783.
27. Matheson, I. B. C. (1990) A critical comparison of least absolute deviation fitting (robust) and least-squares fitting: the importance of error distributions, *Comput. Chem. 14*, 49−57.
28. Johnson, K. A. (1992) in *The Enzymes, 3rd edition, Mechanisms of Catalysis* (Sigman, D. S., Ed.) pp 1−61, Academic Press, New York.
29. Pflugrath, J. W. (1999) The finer things in X-ray diffraction data collection, *Acta Crystallogr. D55*, 1718−1725.
30. Jones, T. A., Zou, J. Y., Cowan, S. W., and Kjelgard, M. (1991) Improved methods for building protein models in electron density maps and the location of errors in these models, *Acta Crystallogr. A47*, 110−119.
31. Sheldrick, G. M., and Schneider, T. R. (1997) SHELXL: High-resolution refinement, *Methods Enzymol. 277*, 319−343.
32. Collaborative Computational Project Number 4 (1994) The CCP4 Suite: Programs for protein crystallography, *Acta Crystallogr. D50*, 760−763.
33. Kraulis, P. J. (1991) MOLSCRIPT: A program to produce both detailed and schematic plots of protein structures, *J. Appl. Crystallogr. 24*, 946−950.
34. Esnouf, R. M. (1997) An extensively modified version of MolScript that includes greatly enhanced coloring capabilities, *J. Mol. Graphics Modell. 15*, 132−134, 112−113.
35. Merritt, E. A., and Murphy, M. E. P. (1994) Raster3D Version 2.0: A program for photorealistic molecular graphics, *Acta Crystallogr. D50*, 869−873.
36. Berglund, G. I., Carlsson, G. H., Smith, A. T., Szoke, H., Henriksen, A., and Hajdu, J. (2002) The catalytic pathway of horseradish peroxidase at high resolution, *Nature 417*, 463−468.
37. Sutin, N., and Yandell, J. K. (1972) Mechanisms of the reactions of cytochrome *c*. Rate and equilibrium constants for ligand binding to horse heart ferricytochrome *c*, *J. Biol. Chem. 247*, 6932−6936.
38. Dumortier, C., Holt, J. M., Meyer, T. E., and Cusanovich, M. A. (1998) Imidazole binding to *Rhodobacter capsulatus* cytochrome c_2. Effect of site-directed mutants on ligand binding, *J. Biol. Chem. 273*, 25647−25653.
39. Sharma, V. S., Traylor, T. G., Gardiner, R., and Mizukami, H. (1987) Reaction of nitric oxide with heme proteins and model compounds of hemoglobin, *Biochemistry 26*, 3837−3843.

BI049748A